CHAPTER 8

ACTIVE GEOPHYSICAL MONITORING OF HYDROCARBON RESERVOIRS USING EM METHODS

Noel Black[a] *and* Michael S. Zhdanov[a]

Contents

1. INTRODUCTION

During recent years marine controlled source electromagnetic (MCSEM) surveys have become intensively used for off-shore petroleum exploration (Eidesmo et al., 2002; Ellingsrud et al., 2002; Carazzone et al., 2005). The importance of MCSEM as an exploration tool is now widely accepted. As the technology advances and the method becomes more affordable, applications other than exploration may find MCSEM data useful. In this paper we study the use of MCSEM methods for reservoir production monitoring.

Effective reservoir management requires time-lapse reservoir information throughout the interwell volume. The ability to understand and control

[a] Department of Geology and Geophysics, University of Utah

Handbook of Geophysical Exploration: Seismic Exploration, Volume 40
ISSN 0950-1401, DOI: 10.1016/S0950-1401(10)04013-9

reservoir behavior over the course of production allows for optimization of reservoir performance and production strategies. Good monitoring information makes it possible to improve the timing and location of new drilling (for both production and injection wells), to recognize flow paths, and to map oil that has been bypassed. The use of seismic data for monitoring is very challenging because of the small variation of seismic velocities over time and because of the difficulty of survey repeatability.

Early investigations of the use of cross-borehole EM data for reservoir monitoring include Malinverno and Torres-Verdín (2000), Hoversten et al. (2001), and Wilt and Morea (2004). Recent sensitivity studies (Lien and Mannseth, 2008; Wang et al., 2008) have assessed the potential of the CSEM technique for reservoir monitoring. Hu et al. (2008) have considered monitoring with array transient electromagnetic (TEM), or time-domain, sounding.

Here, we perform a numerical experiment of reservoir monitoring using MCSEM. We compute EM fields for a model of a partially depleted sea-bottom reservoir with different positions of oil-water contact over time. For a more realistic representation of the sea-bottom environment, we include a salt dome and compare models with and without a rough sea-bottom bathymetry. As an EM modeling tool we use the integral equation (IE)-based code developed at the Consortium for EM Modeling and Inversion (CEMI) at the University of Utah (Hursán and Zhdanov, 2002). We use the multiple-domain (MD) IE method (Endo et al., 2009) to efficiently model extensive anomalous regions of bathymetry, salt structures, and the reservoir itself. Maps of the EM field components clearly reflect the position of the oil-water contact. The principal advantage of the multiple-domain technique is that we are able to isolate the effect of the reservoir. This is especially important in a case where bathymetry must be considered. The oil-water interface is clearly resolved in several field components by extracting only the induction from the reservoir. Our study demonstrates that MCSEM data can accurately provide the position of the oil-water contact inside the reservoir over time.

2. Principles of Reservoir Production Monitoring using Marine EM Methods

EM methods are potentially useful as a means to monitor reservoir production because they can distinguish between hydrocarbons and saline water based on their differing resistivities. The range of resistivity variation is much greater than the range of variation for seismic velocities. Seismic data are useful primarily for estimating lithography and porosity, both of which remain essentially constant over the lifetime of a producing reservoir. Seismic velocities are different enough to discriminate fluid type (oil vs. water) only

for high porosities, greater than about 30%. Since the velocity differences are small, seismic methods rely on fixing survey parameters so that differences between surveys at different points in time can be seen. The potential of seismic methods for monitoring is thus limited by the repeatability of the seismic surveys.

Enhanced oil recovery (EOR) is a prime scenario for investigating the potential use of EM for monitoring. For water injection recovery, there will be a flooding front that advances over time as the reservoir is produced. The ability to locate the position of this oil-water contact is an important test of the method. The main question with EM is resolution. It remains to be seen whether the low frequencies of these methods, which are needed to avoid attenuation to the depths of interest, can resolve the smaller-length scales associated with monitoring compared with those needed for exploration. Since the process is diffusive, there is no applicable Rayleigh criterion limiting expected resolution, and hence a numerical experiment needs to be performed.

3. Overview of the Numerical Modeling Technique

In this section we will present a short overview of the IE method with multiple domains, following Endo et al. (2009). Over the last several years CEMI has developed several computer codes for EM forward modeling based on the integral equation (IE) formulation of Maxwell's equations. In the framework of the IE method, the conductivity distribution is divided into two parts: (1) the background conductivity, σ_b, which is used for the Green's functions calculation, and (2) the anomalous conductivity, $\Delta\sigma_a$, within the domain of integration, D. One principal advantage of the IE method over the other numerical techniques is that the IE method requires discretization of the anomalous domain D only.

The inhomogeneous background conductivity (IBC) IE method (Zhdanov et al., 2006) overcomes the limitation of the conventional IE method of restriction to layered backgrounds only and allows inclusion of important geoelectrical structures like bathymetry and salt domes in the background model. Endo et al. (2009) developed an iterative inhomogeneous IE method for modeling with multiple inhomogeneous domains. By using this method we can evaluate the individual response from every domain, which includes the possible EM coupling effects between the different domains. A rigorous separate calculation of the EM fields produced by different anomalous domains representing different geological structures (e.g., bathymetry, salt structures, reservoirs) is an important practical problem of EM exploration.

The following summarizes the principles of the IE method of EM modeling with multiple inhomogeneous domains. We assume that N inhomogeneous domains ($D_i, i = 1, \ldots, N$) are located within a horizontally layered

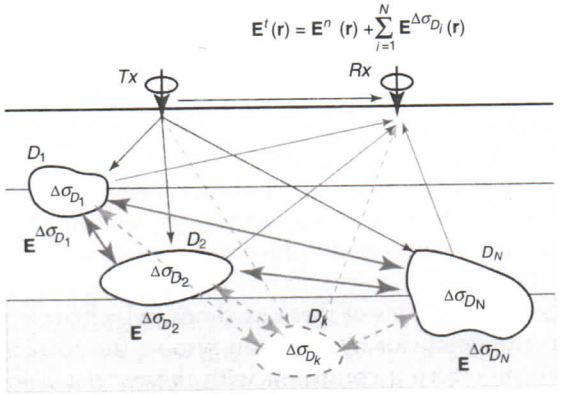

Figure 1 A sketch of a 3D geoelectrical model with horizontally layered (normal) conductivity and N inhomogeneous conductivity domains.

earth (Figure 1). The conductivity of the horizontally layered earth (normal conductivity) is σ_n, while the inhomogeneous (anomalous) conductivity within each inhomogeneous domain is denoted as $\Delta\sigma_{D_i}$, $i = 1, \ldots, N$. The total EM fields at any point $\mathbf{r}$, $\mathbf{E}^t(\mathbf{r})$ and $\mathbf{H}^t(\mathbf{r})$, can be expressed as a sum of the normal fields $\mathbf{E}^n(\mathbf{r})$, $\mathbf{H}^n(\mathbf{r})$, and the EM fields induced by every inhomogeneous domain $\mathbf{E}^{\Delta\sigma_{D_i}}(\mathbf{r})$, $\mathbf{H}^{\Delta\sigma_{D_i}}(\mathbf{r})$ $(i = 1, \ldots, N)$:

$$\mathbf{E}^t(\mathbf{r}) = \mathbf{E}^n(\mathbf{r}) + \sum_{i=1}^{N} \mathbf{E}^{\Delta\sigma_{D_i}}(\mathbf{r}) = \mathbf{E}^n(\mathbf{r}) + \sum_{i=1}^{N} G_E^{D_i}[\Delta\sigma_{D_i}\mathbf{E}^t], \tag{1}$$

$$\mathbf{H}^t(\mathbf{r}) = \mathbf{H}^n(\mathbf{r}) + \sum_{i=1}^{N} \mathbf{H}^{\Delta\sigma_{D_i}}(\mathbf{r}) = \mathbf{H}^n(\mathbf{r}) + \sum_{i=1}^{N} G_H^{D_i}[\Delta\sigma_{D_i}\mathbf{E}^t], \tag{2}$$

where $G_E^{D_i}$ and $G_H^{D_i}$ are electric and magnetic Green's operators acting within domain D_i, respectively. Then the EM modeling problem is reduced to the calculation of the total electric fields inside each inhomogeneous domain.

Rearranging Eq. (1) for the electric field induced in the inhomogeneous domain D_N, we have the following:

$$\mathbf{E}^{\Delta\sigma_{D_N}}(\mathbf{r}) = \mathbf{E}^t(\mathbf{r}) - \mathbf{E}^n(\mathbf{r}) - \sum_{i=1}^{N-1} \mathbf{E}^{\Delta\sigma_{D_i}}(\mathbf{r}). \tag{3}$$

In practice, at the first step of the field calculation, we do not know the values of any electric fields in Eq. (3). We thus first calculate the electric field

in domain D_1 without taking into account the induction effect from any other domains:

$$\mathbf{E}^{\Delta\sigma_{D_1}}(\mathbf{r}) = G_E^{D_1}\left[\Delta\sigma_{D_1}\mathbf{E}^t\right] = \mathbf{E}^t(\mathbf{r}) - \mathbf{E}^n(\mathbf{r}). \tag{4}$$

Equation (4) can be written as an integral equation with respect to the field $E^{\Delta\sigma_{D_1}}$:

$$\mathbf{E}^{\Delta\sigma_{D_1}}(\mathbf{r}) = G_E^{D_1}\left[\Delta\sigma_{D_1}(\mathbf{E}^n + \mathbf{E}^{\Delta\sigma_{D_1}})\right]. \tag{5}$$

This integral equation is solved using the contraction form of the integral equations (Hursán and Zhdanov, 2002) and the complex generalized minimal residual (CGMRES) method (Zhdanov, 2002).

In the calculation of the field due to the currents induced in the next domain (2), we take into account the electric field induced from the inhomogeneous domain D_1, $\mathbf{E}^{\Delta\sigma_{D_1}}(\mathbf{r})$:

$$\mathbf{E}^{\Delta\sigma_{D_2}}(\mathbf{r}) = G_E^{D_2}\left[\Delta\sigma_{D_2}\mathbf{E}^t\right] = \mathbf{E}^t(\mathbf{r}) - \mathbf{E}^n(\mathbf{r}) - \mathbf{E}^{\Delta\sigma_{D_1}}(\mathbf{r}). \tag{6}$$

The last equation is equivalent to the following integral equation:

$$\mathbf{E}^{\Delta\sigma_{D_2}}(\mathbf{r}) = G_E^{D_2}\left[\Delta\sigma_{D_2}(\mathbf{E}^n + \mathbf{E}^{\Delta\sigma_{D_2}} + \mathbf{E}^{\Delta\sigma_{D_1}})\right], \tag{7}$$

which is solved again by the CGMRES method.

Finally, for the last inhomogeneous domain D_N, we already know the electric fields in all the other inhomogeneous domains and thus we can calculate the electric field $\mathbf{E}^{\Delta\sigma_{D_N}}(\mathbf{r})$ as described by Eq. (3).

To improve the accuracy, we can use this scheme iteratively. In the subsequent iterations, we use the fields obtained in the previous iteration to calculate the induced fields in the given domain. For example, in the second iteration, the calculation of the electric fields from the inhomogeneous domain D_N will use the electric fields from other domains obtained in the first iteration as follows:

$$\mathbf{E}_{(2)}^{\Delta\sigma_{D_1}}(\mathbf{r}) = \mathbf{E}_{(1)}^t(\mathbf{r}) - \mathbf{E}^n(\mathbf{r}) - \sum_{i=2}^{N}\mathbf{E}_{(1)}^{\Delta\sigma_{D_i}}(\mathbf{r}), \tag{8}$$

where the numerical field subscripts denote the iteration number. The electric fields from the other inhomogeneous domains are calculated similarly, always using the latest obtained electric fields for the given domain. For example, for the electric fields due to domain D_2 at the second iteration, we

calculate the following:

$$\mathbf{E}_{(2)}^{\Delta\sigma_{D_2}}(\mathbf{r}) = \mathbf{E}_{(1)}^{t}(\mathbf{r}) - \mathbf{E}^{n}(\mathbf{r}) - \sum_{i=3}^{N} \mathbf{E}_{(1)}^{\Delta\sigma_{D_i}}(\mathbf{r}) - \mathbf{E}_{(2)}^{\Delta\sigma_{D_1}}(\mathbf{r}). \tag{9}$$

This process is repeated until the electric fields within all the inhomogeneous domains reach self-consistency, i.e., the norm of difference between the electric fields in any domain at iterations i and $(i-1)$ is less than a certain threshold ε. In the kth inhomogeneous domain, for example, the electric fields satisfy the following inequality:

$$\frac{\left\| \mathbf{E}_{(i)}^{\Delta\sigma_{D_k}}(\mathbf{r}_j) - \mathbf{E}_{(i-1)}^{\Delta\sigma_{D_k}}(\mathbf{r}_j) \right\|_2}{\left\| \mathbf{E}_{(i)}^{\Delta\sigma_{D_k}}(\mathbf{r}_j) \right\|_2} < \varepsilon, \quad r_j \in D_k. \tag{10}$$

4. Computer Simulation of HC Reservoir Monitoring using EM Methods

We will perform a numerical experiment of forward modeling for several stages in the production of a reservoir by water injection. We consider a realistic geoelectric model of an HC reservoir and accompanying salt dome, first without and then with a sea-bottom bathymetry. The reservoir is filled from one end with injected saline water. For simplicity we model the oil-water contact as a sharp vertical interface. The EM field is generated by horizontal electric bipoles near the seafloor and detected by a line of receivers at the seafloor. The models are described in more detail in the following sections.

4.1. Model 1: HC reservoir and a salt dome structure

A vertical section of the geoelectric structure of Model 1 is shown in Figure 2. This figure shows a resistive HC reservoir with a resistivity of 100 Ohm m and a salt dome with a resistivity of 30 Ohm m located within conductive sea-bottom sediments whose resistivity is 1 Ohm m. The resistivity of the seawater layer is 0.33 Ohm m, and the depth of the seafloor is 1350 m below sea level. The reservoir is flooded from the right (positive x direction) by water having a resistivity of 0.5 Ohm m. We model four positions (x_0 = 14.0, 12.8, 11.6, and 10.4 km) of the (vertical) oil-water interface to simulate production.

The EM field in this model is excited by an x-directed horizontal electric bipole of length 1 m and current 1000 A, which is located at the points with horizontal coordinates from 0 to 20 km (every 200 m) in the x direction and

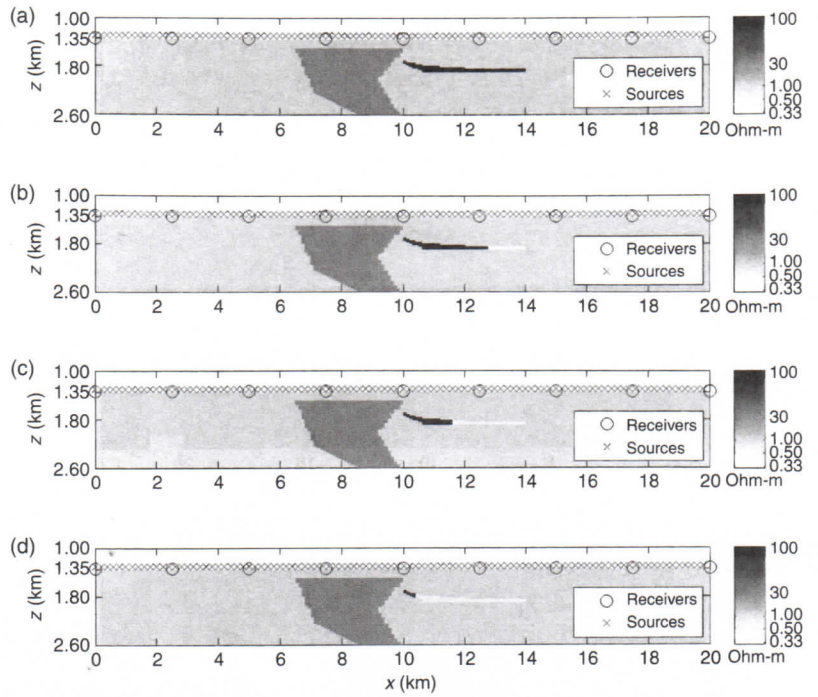

Figure 2 A vertical geoelectrical section of Model 1, containing a salt dome and a reservoir.

from −3 km to 3 km (every 200 m) in the y direction. The elevation of the transmitter bipole is 50 m above the sea bottom. The transmitter generates the frequency-domain EM field at frequencies of 0.01 Hz and 0.3162 Hz (we studied a range of frequencies between 0.01 and 10.0 Hz, and present results for these two). We modeled nine electric field receivers, equally spaced (2.5 km spacing) along the y axis between 0 and 20 km. To narrow the scope we confine our analysis in this paper to the first source at the far left of Figure 2 ($x = 0$).

Following the main principles of the MD IE method for multiple inhomogeneous domains, the modeling area is divided into two modeling domains, D_1 and D_2, corresponding to the locations of the salt dome and HC reservoir, respectively. Domain D_1 for the salt dome area is discretized into $35 \times 60 \times 10 = 36{,}960$ cells with a cell size of $100 \times 100 \times 25$ m^3, and domain D_2 for the HC reservoir area is discretized into $40 \times 40 \times 8 = 12{,}9800$ cells with the same cell size, $100 \times 100 \times 25$ m^3.

4.2. Model 1: Forward modeling results

Figures 3 and 4 show the x (in-line) component of the total electric field normalized by the fields induced in the layered background and the salt

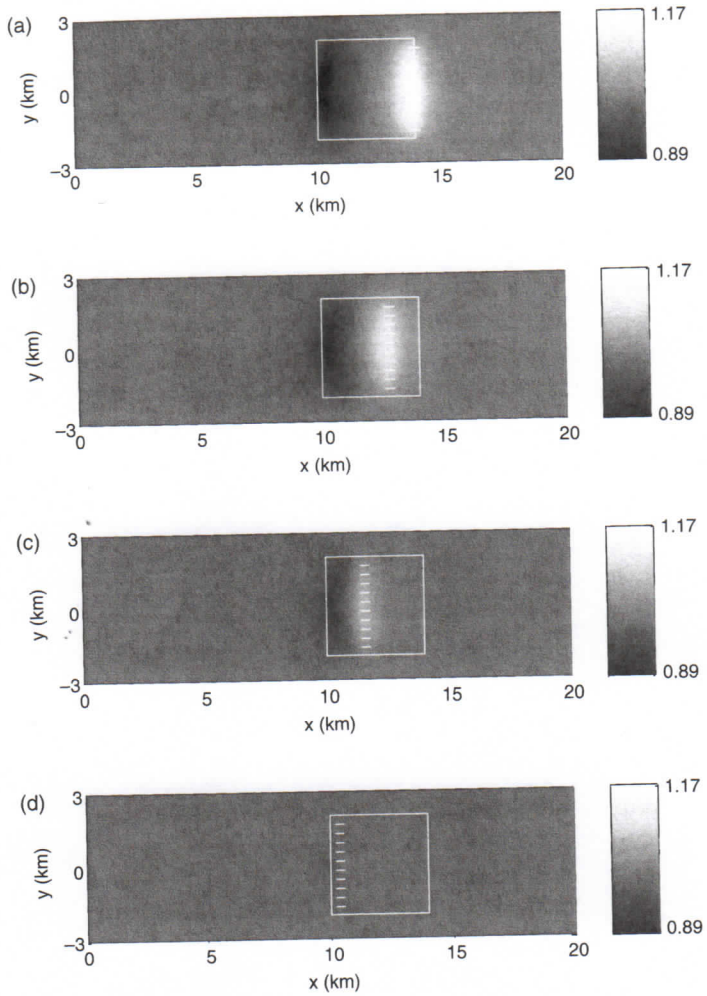

Figure 3 $|E_x^{\text{tot}}|$ normalized by background and salt dome fields for frequency = 0.01 Hz.

dome, $|E_x^{\text{tot}}| / (|E_x^b| + |E_x^{sd}|)$, for the sea-bottom receiver #1 (located at $x = 0$ km) and for the transmitter frequencies 0.01 Hz (Figure 3) and 0.3162 Hz (Figure 4). The higher frequency produces greater resolution and contrast but a smaller total field. The solid white box indicates the horizontal position of the reservoir, and the dashed white line indicates the horizontal position x_0 of the oil-water interface for four different positions (i.e., stages of production). Water fills from the right (positive x direction), forcing the oil to the left (negative x direction). The interface is clearly seen for all four positions as an enhancement of the normalized field component.

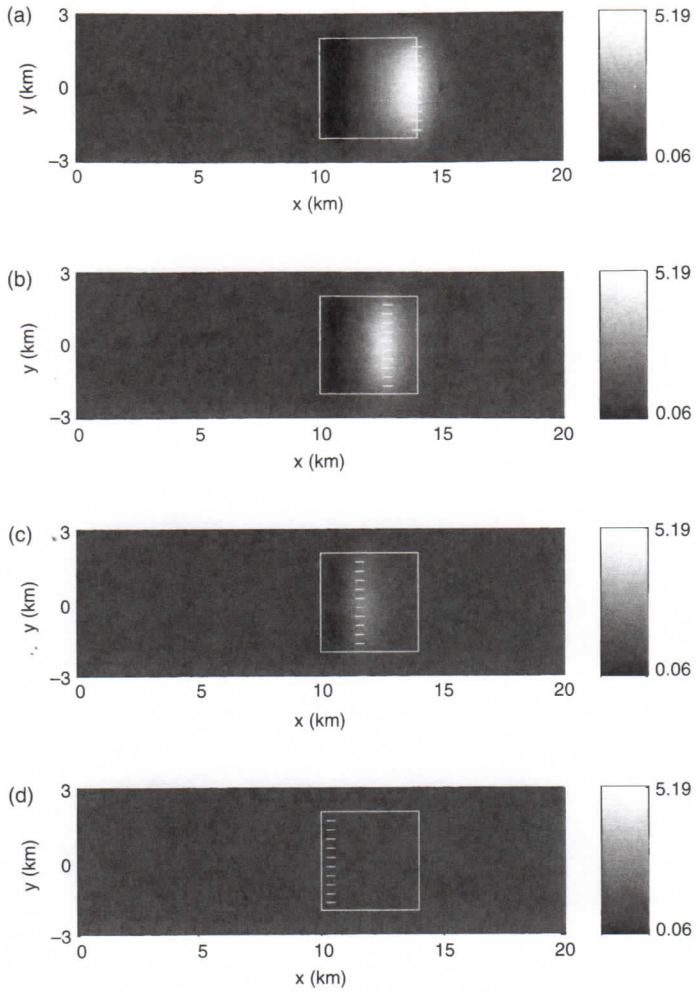

Figure 4 $|E_x^{\text{tot}}|$ normalized by background and salt dome fields for frequency = 0.3162 Hz.

Figures 5 and 6 show the same but normalized by the layered background field only $\left(|E_x^{\text{tot}}| / |E_x^b|\right)$. The salt dome location is now seen, as is the left (negative x) boundary of the HC reservoir.

Figures 7 and 8 show the z (vertical) component of the total electric field normalized by the fields induced in the layered background and the salt dome, $|E_z^{\text{tot}}| / \left(|E_z^b| + |E_z^{sd}|\right)$, for the sea-bottom receiver #1 (compare with Figures 3 and 4 for the x component). The location of the HC reservoir and the oil-water interface is clearly seen for the lower frequency as a negative anomaly. The unproduced portion of the reservoir is nicely

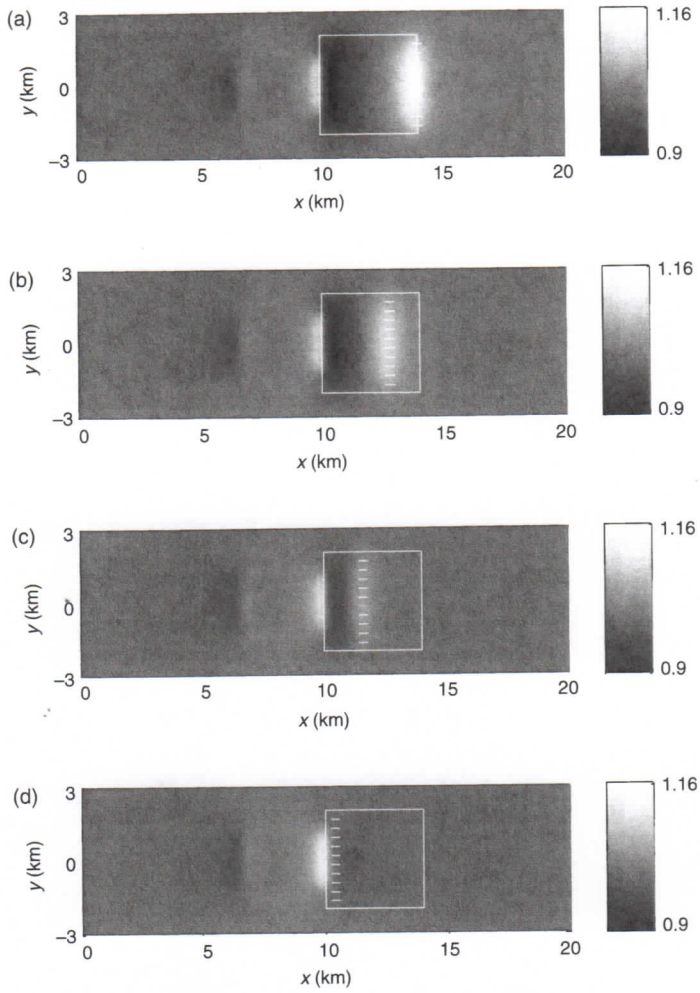

Figure 5 $|E_x^{\text{tot}}|$ normalized by background field for frequency = 0.01 Hz.

outlined in the higher frequency plot by a positive anomalous field along its boundary. For both frequencies, we can clearly see not only the oil-water contact but also the location of the remaining hydrocarbon.

The magnitude of the x and z electric field components of the source-moment-normalized anomalous reservoir electric field is in the range of 10^{-14}-10^{-15} V/m. This is slightly above, or approximately at, the noise level of 10^{-15} V/m set by Um and Alumbaugh (2007). This noise estimate is slightly higher than that given by Constable and Weiss (2006). The anomalous reservoir response is therefore expected to be detectable.

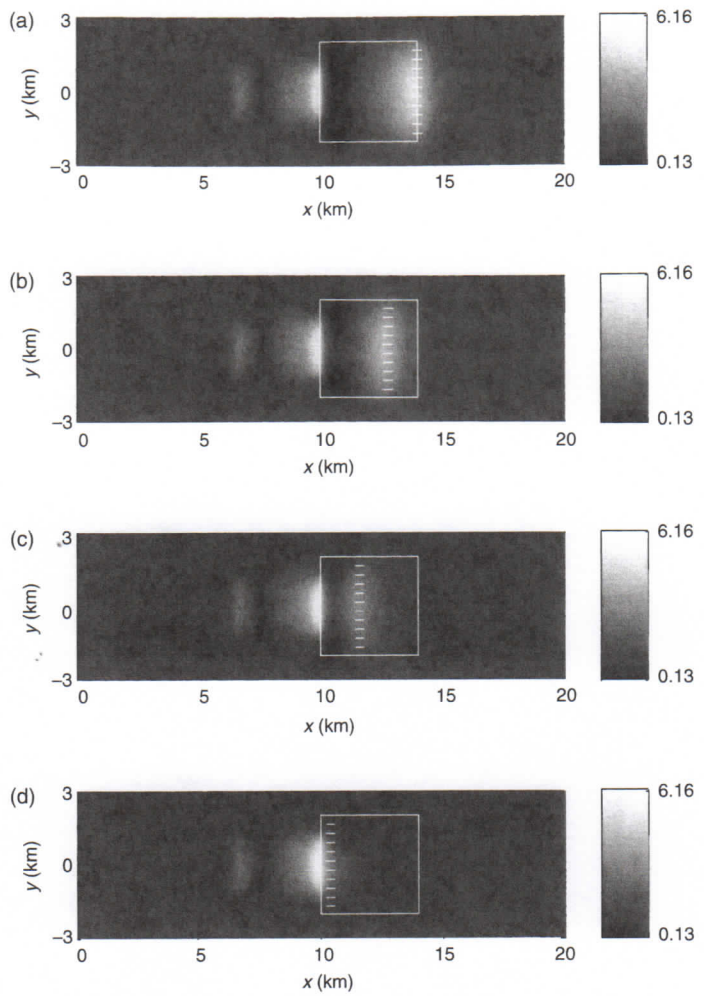

Figure 6 $|E_x^{\text{tot}}|$ normalized by background field for frequency = 0.3162 Hz.

4.3. Model 2: HC reservoir and a salt dome in an area with a rough sea-bottom bathymetry

In this section we study the feasibility of identifying the location of the oil-water interface from MCSEM data in a case where there is a rough sea-bottom bathymetry. This is very important from a practical standpoint because the effect of the bathymetry can significantly distort the EM response from an HC reservoir, and therefore the oil-water interface position in production monitoring can also be affected by the bathymetry. As a prototype of the bathymetry structure we use a simplified model of the known

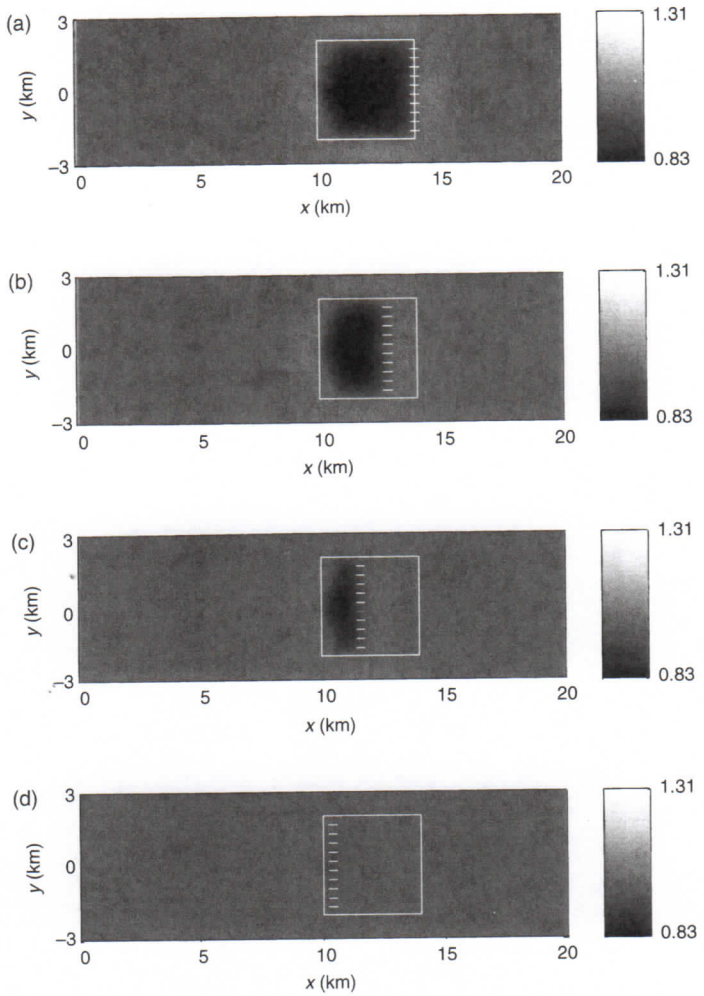

Figure 7 $|E_z^{\text{tot}}|$ normalized by background and salt dome fields for frequency = 0.01 Hz.

bathymetry of the Sabah area, Malaysia (provided by Shell International Exploration and Production, acquired in 2004). A vertical section of the model is shown in Figure 9. It includes three domains: D_1 for the bathymetry discretized as $200 \times 60 \times 10 = 120{,}000$ cells, and domains D_2 for the salt dome and D_3 for the HC reservoir, discretized as in Model 1.

4.4. Model 2: Forward modeling results

Figures 10 and 11 show the x (in-line) component of the total electric field normalized by the fields induced in the layered background, bathymetry, and

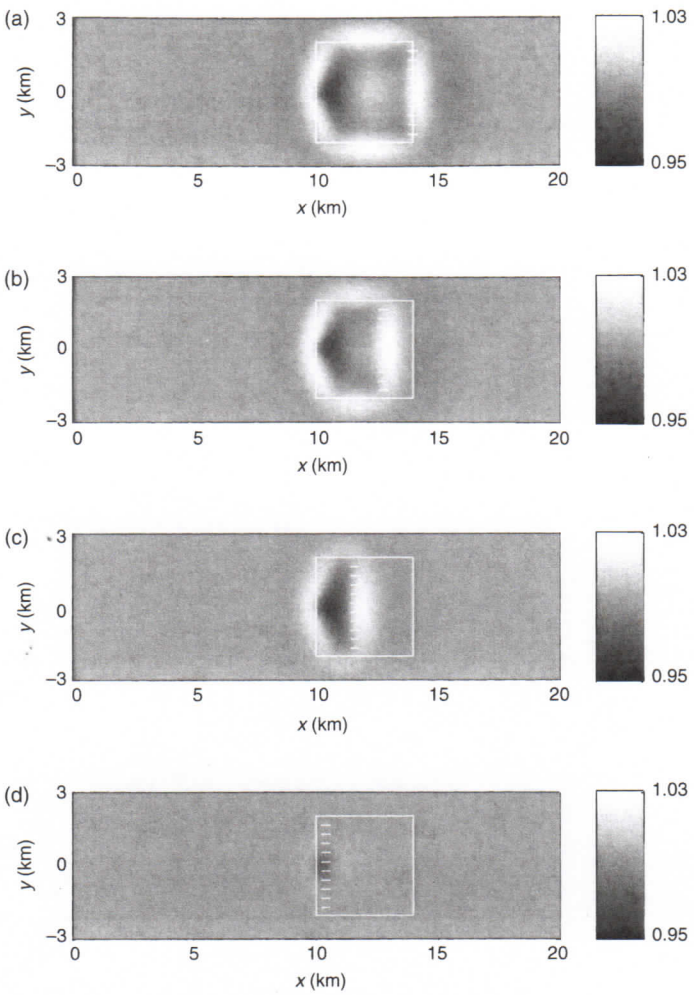

Figure 8 $|E_z^{\text{tot}}|$ normalized by background and salt dome fields for frequency = 0.3162 Hz.

the salt dome $|E_x^{\text{tot}}| / (|E_x^b| + |E_x^{\text{bath}}| + |E_x^{sd}|)$ for the sea-bottom receiver #1 and for both frequencies. The position of the oil-water contact is again seen as an enhancement in the field. The anomalous field from the reservoir is slightly less pronounced when a bathymetry is present, but this is not a large effect.

Figures 12 and 13 show the same electric field component normalized by the background and bathymetry fields. Again, the location of the salt dome is now revealed; the oil-water contact is still clearly seen although its anomalous response is somewhat suppressed compared to the first normalization, which includes the salt dome.

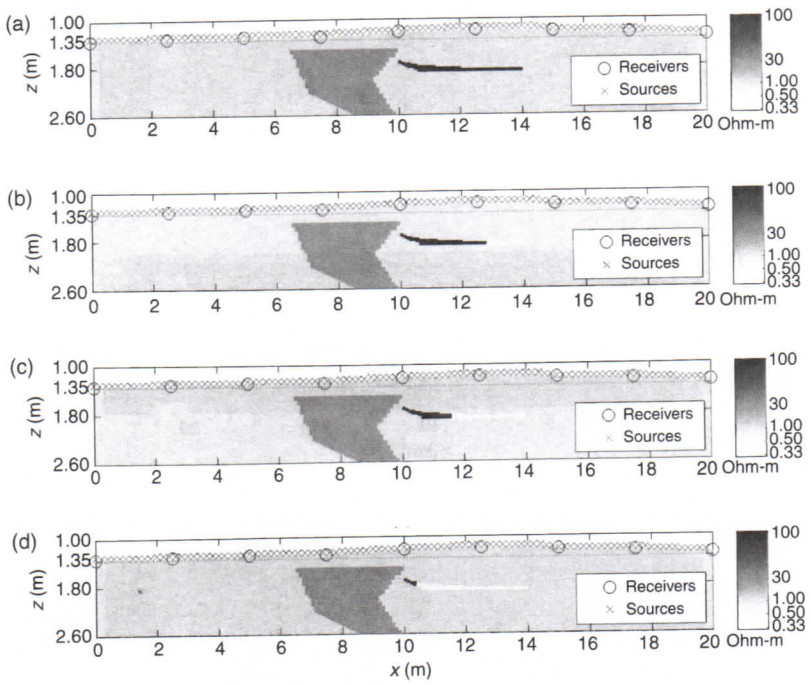

Figure 9 A vertical geoelectrical section of Model 2, containing a salt dome and a reservoir with a sea-bottom bathymetry.

Similar results were obtained for the z component of the electric field (Figures 14 and 15) to those obtained without a sea-bottom bathymetry. The unproduced portion of the reservoir and in particular the oil-water contact are clearly seen with only a slightly less pronounced anomalous field compared to the case without bathymetry.

Figures 16 and 17 show the y component of the magnetic field for the two frequencies under consideration. The results are similar to those for the x component of the electric field, showing the oil-water contact position very nicely. Figures 18 and 19 show the x component of the magnetic field, with results similar to the z component of the electric field. The remaining hydrocarbon can be seen, and in particular the oil-water contact location is clearly demarked.

The magnitude of the x and y magnetic field components of the source-moment-normalized anomalous reservoir magnetic field is in the range 10^{-8}-10^{-11} nT/m. The noise level quoted by Um and Alumbaugh (2007) is 10^{-10} nT/m. We therefore expect that at least some of these components will be detectable for the survey parameters modeled here.

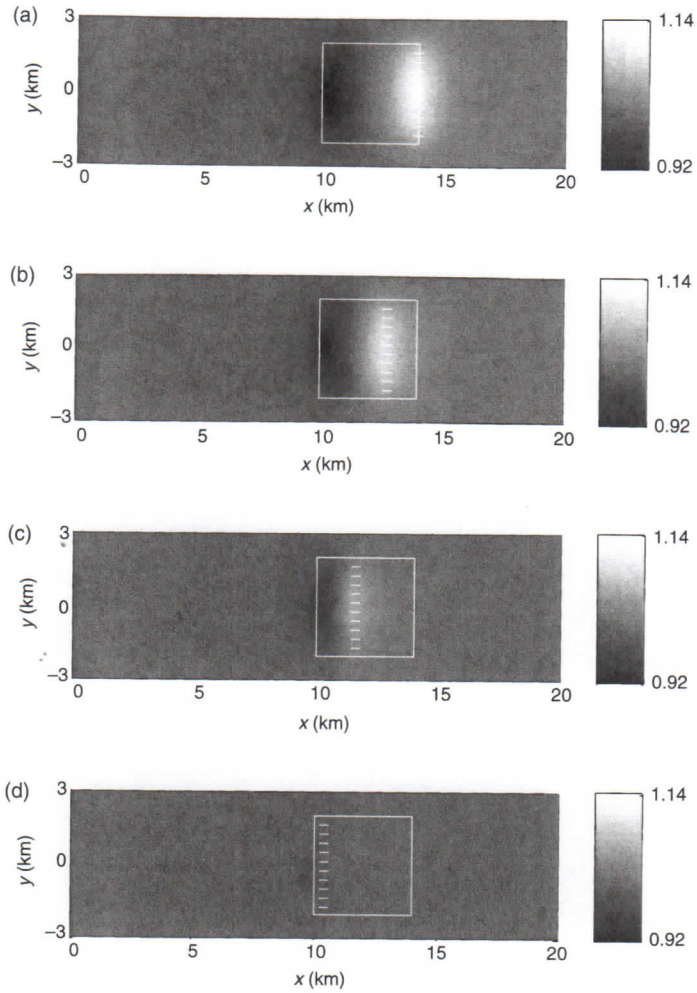

Figure 10 $|E_x^{\text{tot}}|$ normalized by background, bathymetry, and salt dome fields for frequency = 0.01 Hz.

5. CONCLUSIONS

The difference in the resistivities of the oil and the water filling the reservoir during production allows the possibility of monitoring the flooding front by EM methods. The oil-water interface can be clearly seen in several field components, even with a sea-bottom bathymetry. Induction due to the different anomalous domains can be extracted separately with the IBC method, allowing for different normalizations of the total field. The reservoir, and therefore the oil-water contact, can be seen most clearly when normalized by the background, bathymetry, and salt dome fields.

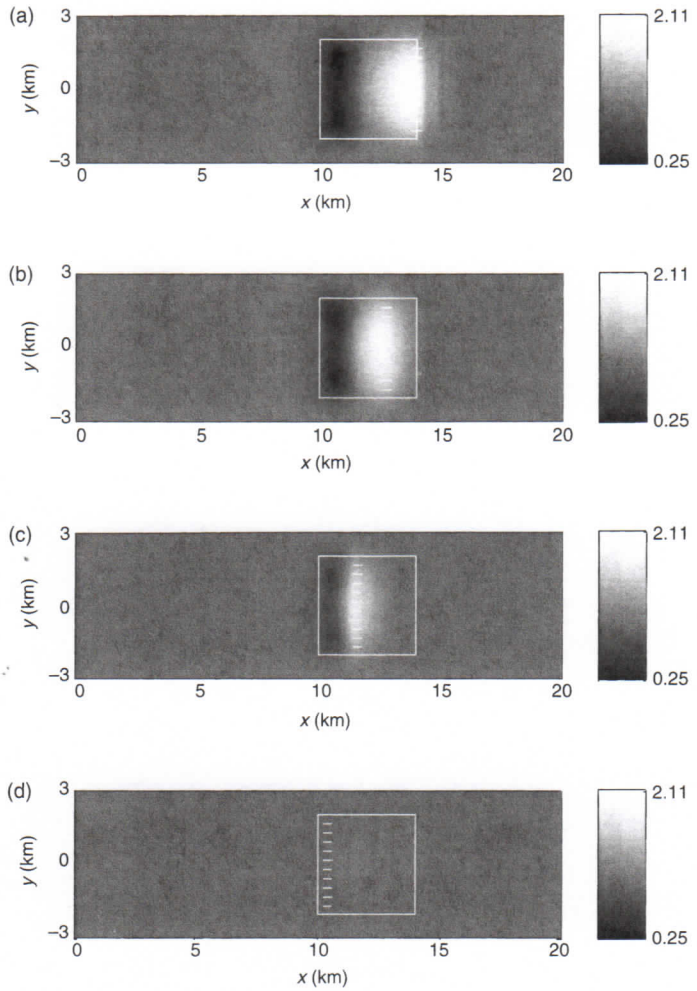

Figure 11 $|E_x^{\text{tot}}|$ normalized by background, bathymetry, and salt dome fields for frequency = 0.3162 Hz.

Our study demonstrates that measurable MCSEM data can provide an accurate position of the oil-water contact inside the reservoir over time. Future work should study more realistic models of the flooding front in the water injection recovery method. The oil-water interface can be nonvertical (angled), it can be nonsharp (occurring as a transition zone of up to tens of meters thick), and we should consider flooding from the bottom. Injection water of a range of resistivities should also be studied. The positive results of our experiment here, with a simplified flooding scheme (but a realistic geological model), warrant these further investigations into the use of EM methods for reservoir monitoring during production.

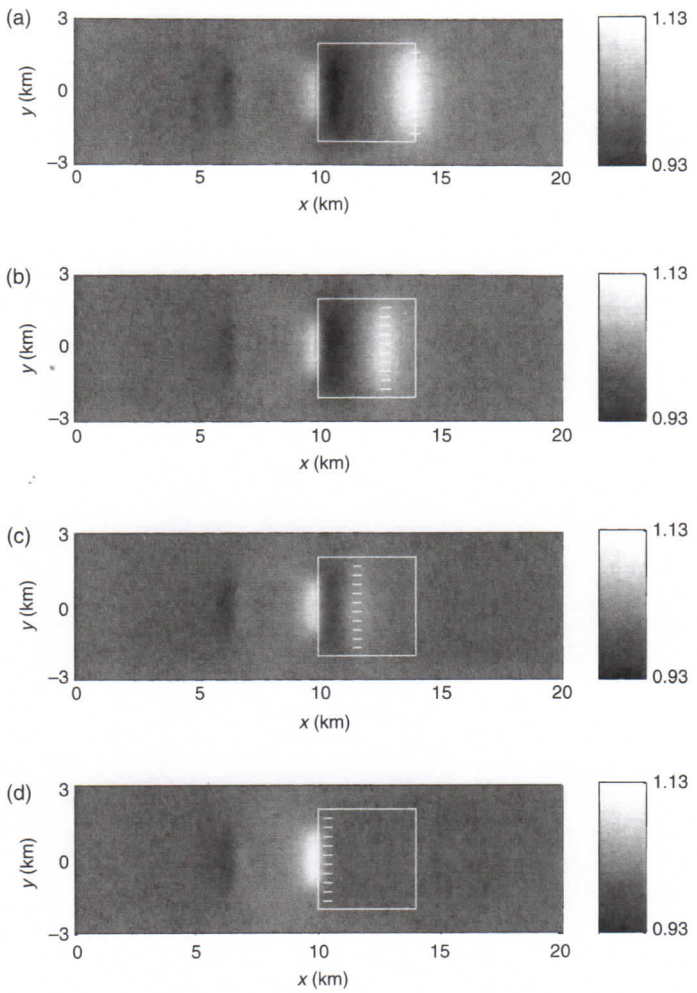

Figure 12 $|E_x^{\text{tot}}|$ normalized by background and bathymetry fields for frequency = 0.01 Hz.

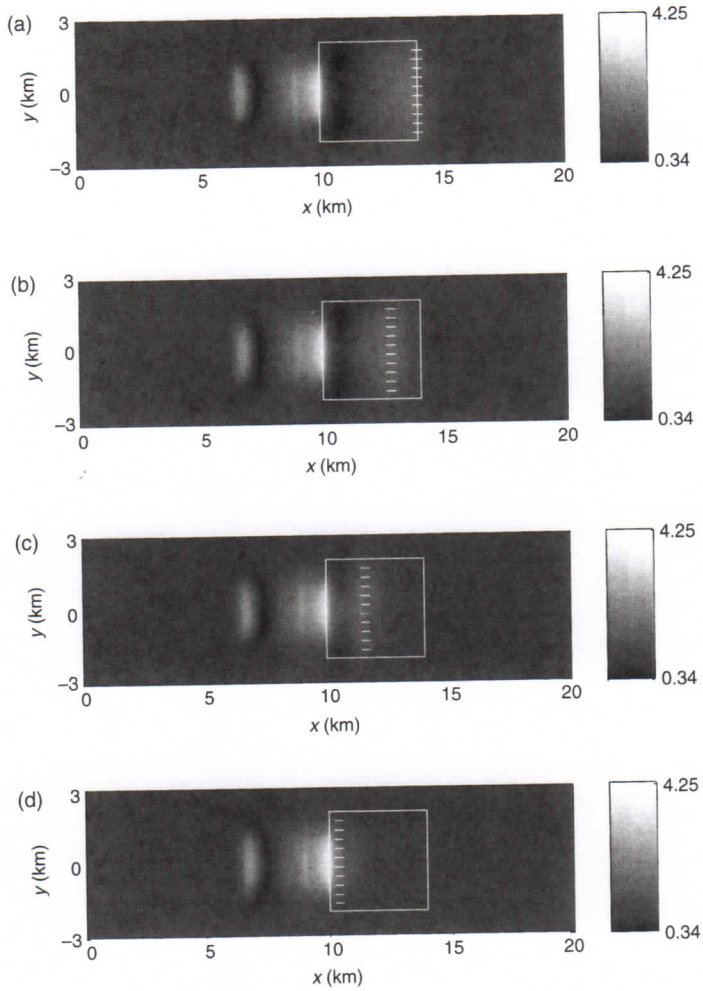

Figure 13 $|E_x^{\text{tot}}|$ normalized by background and bathymetry fields for frequency = 0.3162 Hz.

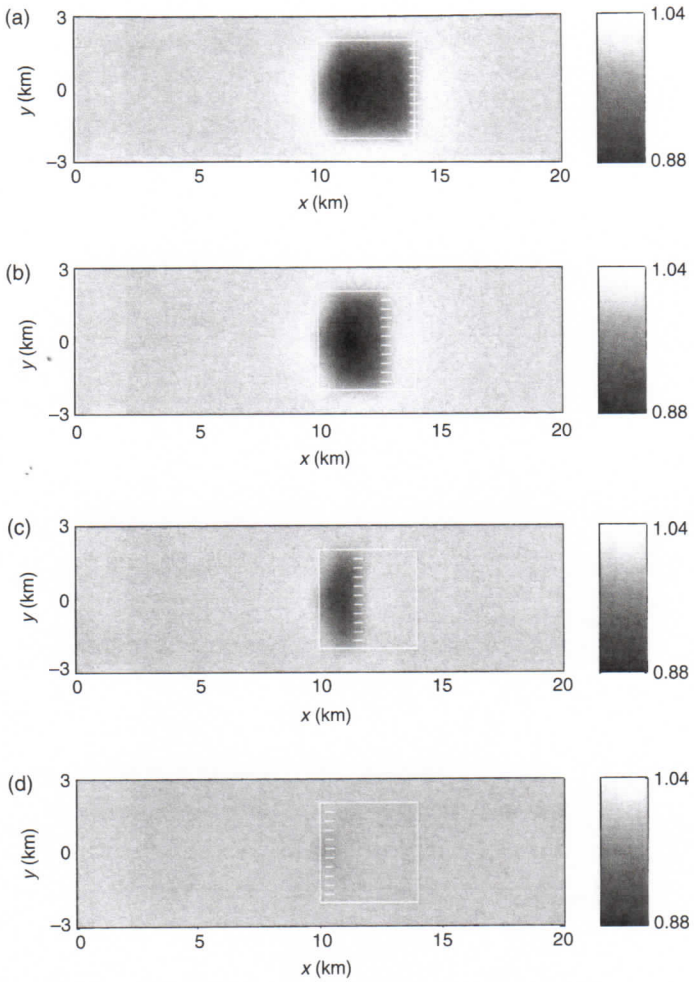

Figure 14 $|E_z^{\text{tot}}|$ normalized by background, bathymetry, and salt dome fields for frequency = 0.01 Hz.

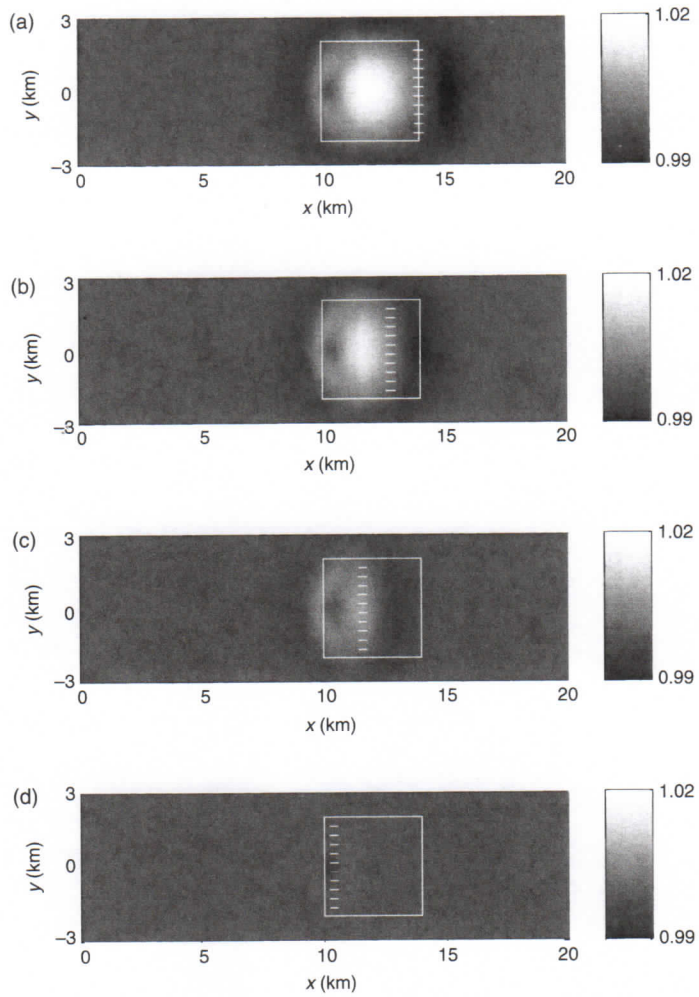

Figure 15 $|E_z^{\text{tot}}|$ normalized by background, bathymetry, and salt dome fields for frequency = 0.3162 Hz.

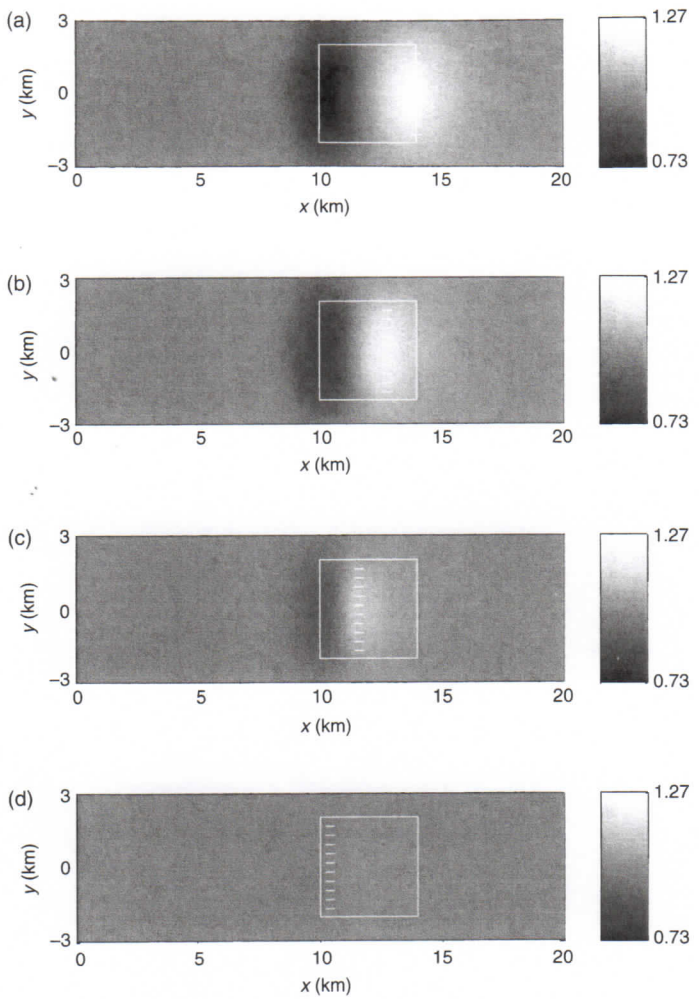

Figure 16 $\left|H_y^{\text{tot}}\right|$ normalized by background, bathymetry, and salt dome fields for frequency = 0.01 Hz.

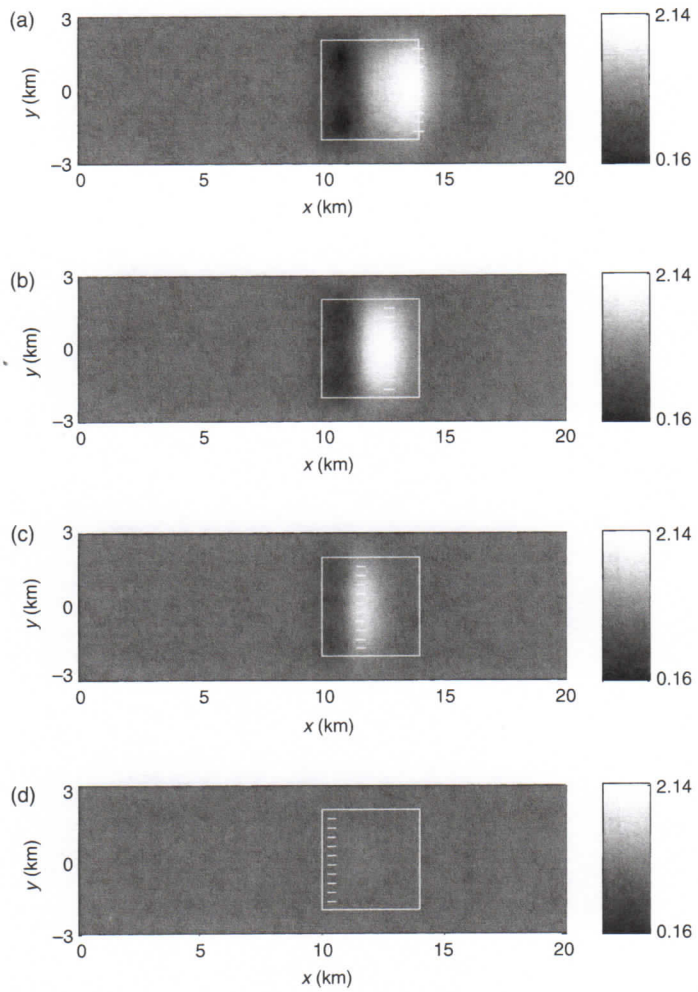

Figure 17 $\left|H_y^{\text{tot}}\right|$ normalized by background, bathymetry, and salt dome fields for frequency = 0.3162 Hz.

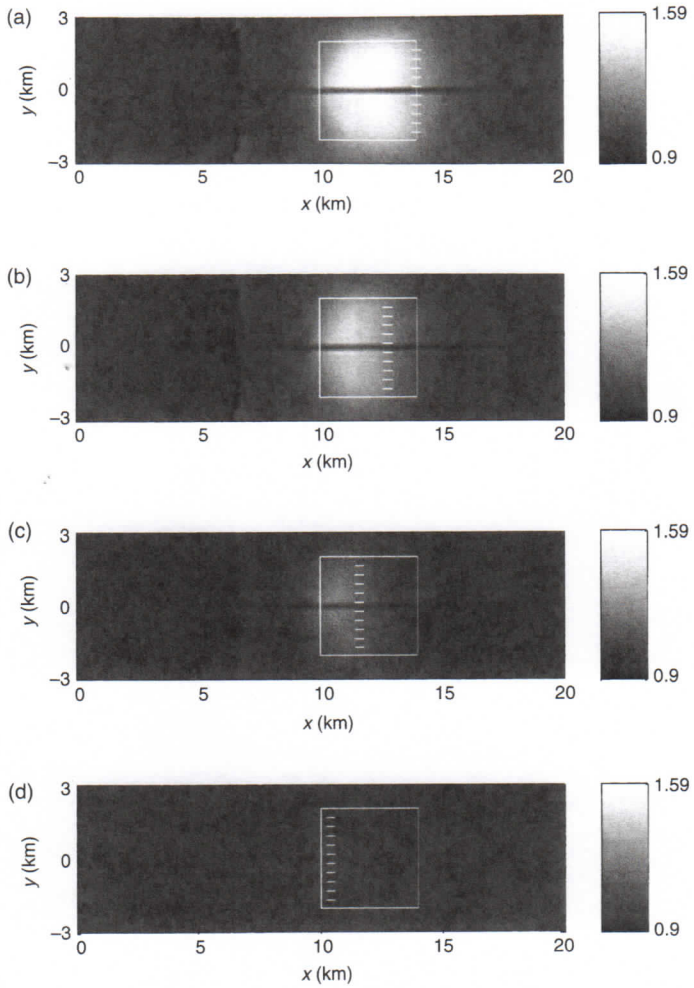

Figure 18 $|H_x^{\text{tot}}|$ normalized by background, bathymetry, and salt dome fields for frequency = 0.01 Hz.

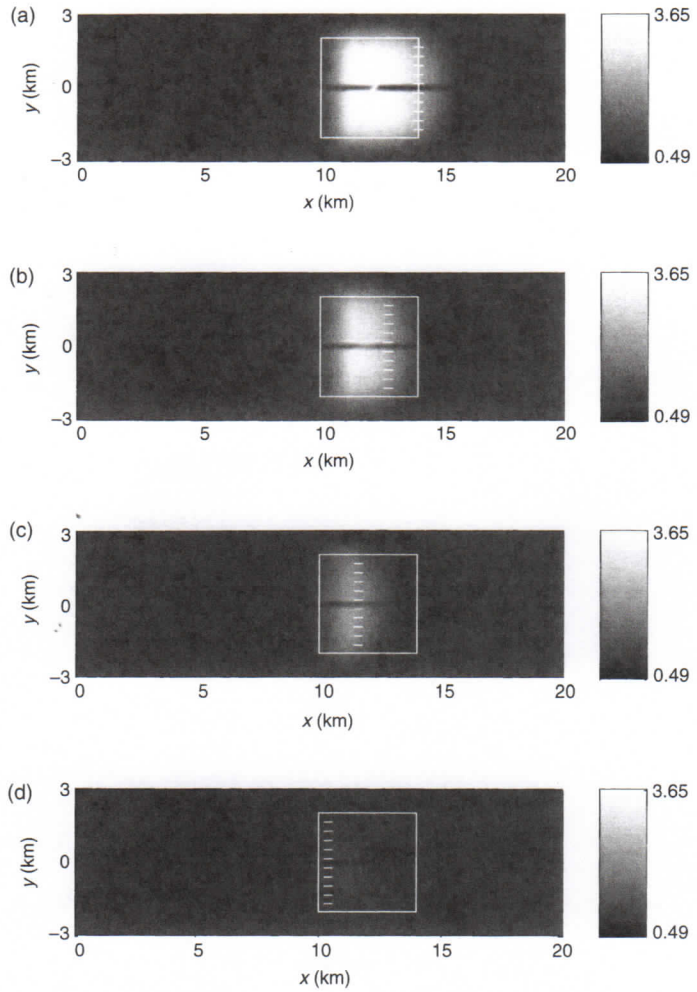

Figure 19 $|H_x^{\text{tot}}|$ normalized by background, bathymetry, and salt dome fields for frequency = 0.3162 Hz.

ACKNOWLEDGMENTS

The authors acknowledge the support of the University of Utah Consortium for Electromagnetic Modeling and Inversion (CEMI), which includes BAE Systems, Baker Atlas Logging Services, BGP China National Petroleum Corporation, BHP Billiton World Exploration Inc., BP, EMGS, ENI S.p.A., ExxonMobil Upstream Research Company, Fugro, Halliburton Energy Services, Information Systems Laboratories, Newmont Mining Co., OHM, Petrobras, PGS, Rio Tinto - Kennecott, Rocksource, Russian

Research Center Kurchatov Institute, Schlumberger, Science Applications International Co., Shell International Exploration and Production Inc., StatoilHydro, Sumitomo Metal Mining Co., Woodside Energy, and Zonge Engineering and Research Organization.

REFERENCES

Carazzone, J.J., Burtz, O.M., Green, K.E., Pavlov, D.A., 2005. Three dimensional imaging of marine CSEM data. In: 75th Annual International Meeting, SEG, Expanded Abstracts, pp. 575–578.

Constable, S., Weiss, C.J., 2006. Mapping thin resistors and hydrocarbons with marine EM methods: Insight from 1D modeling. Geophysics 71 (2), G43–G51.

Eidesmo, T., Ellingsrud, S., MacGregor, L.M., Constable, S., Sinha, M.C., Johansen, S., Kong, F.N., Westerdahl, H., 2002. Sea bed logging (SBL), a new method for remote and direct identification of hydrocarbon filled layers in deepwater areas. First Break 20, 144–152.

Ellingsrud, S., Eidesmo, T., Johansen, S., Sinha, M.C., MacGregor, L.M., Constable, S., 2002. Remote sensing of hydrocarbon layers by seabed logging (SBL): Results from a cruise offshore Angola. The Leading Edge 21, 972–982.

Endo, M., Cuma, M., Zhdanov, M.S., 2009. Large-scale electromagnetic modeling for multiple inhomogeneous domains. Communications in Computational Physics 6, 269–289.

Hoversten, G.M., Newman, G.A., Morrison, H.F., Gasperikova, E., 2001. Reservoir characterization using crosswell electromagnetic inversion: A feasibility study for the Snorre field, North Sea. Geophysics 66, 1177–1189.

Hu, W., Yan, L., Su, Z., Zheng, R., Strack, K., 2008. Array TEM sounding and application for reservoir monitoring. In: 78th Annual International Meeting, SEG, Expanded Abstracts, pp. 634–638.

Hursán, G., Zhdanov, M.S., 2002. Contraction integral equation method in three-dimensional electromagnetic modeling. Radio Science 37, 1089–2002.

Lien, M., Mannseth, T., 2008. Sensitivity study of marine CSEM data for reservoir production monitoring. Geophysics 73, F151–F163.

Malinverno, A., Torres-Verdín, C., 2000. Bayesian inversion of DC electrical measurements with uncertainties for reservoir monitoring. Inverse Problems 16, 1343–1356.

Um, E.S., Alumbaugh, D.L., 2007. On the physics of the marine controlled-source electromagnetic method. Geophysics 72, WA13–WA26.

Wang, Z., Gelius, L., Kong, F., 2008. A sensitivity analysis of the sea bed logging technique with respect to reservoir heterogeneities. In: 78th Annual International Meeting, SEG, Expanded Abstracts, pp. 711–715.

Wilt, M., Morea, M., 2004. 3D waterflood monitoring at Lost Hills with crosshole EM. The Leading Edge 23, 489–493.

Zhdanov, M.S., 2002. Geophysical inverse theory and regularization problems. Elsevier.

Zhdanov, M.S., Lee, S.K., Yoshioka, K., 2006. Integral equation method for 3D modeling of electromagnetic fields in complex structures with inhomogeneous background conductivity. Geophysics 71, G333–G345.